

# Light: A Scalable and Efficient Wavelength-Routed Optical Networks-On-Chip Topology

Zhidan Zheng, Mengchu Li, Tsun-Ming Tseng, and Ulf Schlichtmann

{zhidan.zheng,mengchu.li,tsun-ming.tseng,ulf.schlichtmann}@tum.de

Chair of Electronic Design Automation, Technical University of Munich, Munich, Germany

## ABSTRACT

Wavelength-routed optical networks-on-chip (WRONoCs) are known for delivering collision- and arbitration-free on-chip communication in many-cores systems. While appealing for low latency and high predictability, WRONoCs are challenged by scalability concerns due to two reasons: (1) State-of-the-art WRONoC topologies use a large number of microring resonators (MRRs) which result in much MRR tuning power and crosstalk noise. (2) The positions of master and slave nodes in current topologies do not match realistic layout constraints. Thus, many additional waveguide crossings will be introduced during physical implementation, which degrades the network performance. In this work, we propose an  $N \times (N - 1)$  WRONoC topology: *Light* with a  $4 \times 3$  router *Hash* as the basic building block, and a simple but efficient approach to configure the resonant wavelength for each MRR. Experimental results show that *Light* outperforms state-of-the-art topologies in terms of enhancing signal-to-noise ratio (SNR) and reducing insertion loss, especially for large-scale networks. Furthermore, *Light* can be easily implemented onto a physical plane without causing external waveguide crossings.

## ACM Reference Format:

Zhidan Zheng, Mengchu Li, Tsun-Ming Tseng, and Ulf Schlichtmann. 2021. Light: A Scalable and Efficient Wavelength-Routed Optical Networks-On-Chip Topology. In *26th Asia and South Pacific Design Automation Conference (ASPDAC '21)*, January 18–21, 2021, Tokyo, Japan. ACM, New York, NY, USA, 7 pages. <https://doi.org/10.1145/3394885.3431613>

## 1 INTRODUCTION

Stimulated by recent breakthroughs in silicon photonics, optical networks-on-chip (ONoCs) emerge as a next-generation solution to keep up with the ever-increasing on-chip communication in multiprocessor system-on-chip (MPSoC) [3]. Taking advantage of the wavelength-division multiplexing (WDM) technology and the ultra-low propagation delay of light in silicon, ONoCs promise to offer much higher bandwidth with much lower latency compared to conventional electronic NoCs.

Current ONoC architectures can be classified into two categories: *control-networks-based* and *wavelength-routed* [17]. On control-networks-based ONoCs, before a sender (master) can transmit data to a receiver (slave), a signal path needs to be reserved through

Permission to make digital or hard copies of all or part of this work for personal or classroom use is granted without fee provided that copies are not made or distributed for profit or commercial advantage and that copies bear this notice and the full citation on the first page. Copyrights for components of this work owned by others than ACM must be honored. Abstracting with credit is permitted. To copy otherwise, or republish, to post on servers or to redistribute to lists, requires prior specific permission and/or a fee. Request permissions from [permissions@acm.org](mailto:permissions@acm.org).

ASPDAC 2021, DOI: [10.1145/3394885.3431613](https://doi.org/10.1145/3394885.3431613)  
<https://ieeexplore.ieee.org/document/9371649>  
<https://dl.acm.org/doi/10.1145/3394885.3431613>



Figure 1: Working mechanism in CSEs

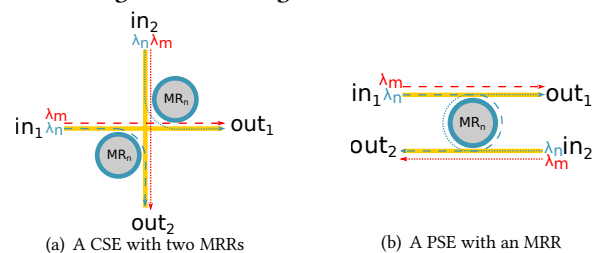


Figure 2: Optical Switching Elements

an additional control network [4, 16]. To avoid data collision, only one master-slave pair is allowed to communicate at any given time. Wavelength-routed ONoCs (WRONoCs), on the other hand, fix collision-free signal paths between all master-slave pairs at design time and are thus free from the energy and latency overhead for arbitration [1, 2, 11]. With a set of different wavelengths, all masters can communicate to all their slaves concurrently.

On WRONoCs, optical signals are routed passively based on their wavelengths by silicon microring resonators (MRRs). An MRR consists of a looped optical waveguide, i.e. the microring (MR), and a coupling mechanism to access the microring [12, 19]. When an optical signal approaches an MRR, if the wavelength of the signal matches the resonant wavelength of the MRR, the signal will be *on-resonance* with the MRR and coupled to the microring; otherwise, the signal will be *off-resonance* with the MRR and pass it without being affected [18].

State-of-the-art WRONoC topologies such as  $\lambda$ -router [10], GWOR [20] and Snake [8] are mostly built upon crossing switching elements (CSEs), where MRRs are placed near waveguide crossings to distribute signals on different wavelengths to their designated paths. As shown in Figure 1(a) and Figure 1(b), based on the input direction of an optical signal, a CSE can support either 90-degree or 270-degree direction change of the signals. However, since the 270-degree signal path generates much more insertion loss and crosstalk noise, most researchers prefer to only employ the 90-degree routing mechanism and implement a CSE with two identical MRRs, as shown in Figure 2(a) [9, 22].

A problem of the WRONoC topologies that employ CSEs with two MRRs is their high MRR usage. For example, for the network with 64 IP-cores, 4032 MRRs are used in  $\lambda$ -router, and 3968 MRRs are used in GWOR. The high MRR usage challenges the system performance, since it results in much MRR tuning power and crosstalk

noise [5]. Thus, reducing the MRR usage becomes one of the most urgent problems in WRONoC topology design.

Besides MRR usage, another major concern about current WRONoC topologies is their mismatch with physical layout constraints. State-of-the-art topologies usually treat masters and slaves as unrelated nodes and put them at two distant ends of the logic scheme [8, 10]. However, when we consider realistic WRONoC applications such as 3D-integrated many-cores systems [7, 15], each IP-core actually both sends and receives data, which means that it acts as both master and slave. Thus, instead of being far away from each other, the positions of the master and the slave that represent the same IP-core should be very close. The separation of masters and slaves in state-of-the-art topologies leads to additional waveguide crossings during physical implementation. For example, while an  $8 \times 8$   $\lambda$ -router only has 28 waveguide crossings in its logic scheme, there are 64 crossings in its physical one [6], which indicates a significant rise of the insertion loss and crosstalk noise.

In this paper, we propose a novel  $4 \times 3$  router structure: *Hash*, which looks like a hash mark and uses parallel switching elements (PSEs) for wavelength routing. In a PSE, an MRR is placed between two parallel waveguides so that signals entering the PSE will experience a 180-degree direction change, as shown in Figure 2(b). Thus, a  $2 \times 2$  PSE that supports two input and two output ports can be implemented with only one MRR without introducing much insertion loss or crosstalk noise. Based on Hash, we propose a novel WRONoC topology: *Light*, which concurrently supports  $N \times (N - 1)$  communication at any scale with a straightforward resonant wavelength configuration approach. Compared to the typical state-of-the-art topologies, *Light* reduces the number of MRRs by more than half and shows significant advantages in energy efficiency and signal quality. Regardless of the number and the positions of the IP-cores, *Light* can always be physically implemented without causing additional waveguide crossings or detour.

The rest of the paper is organized as follows. Section 2 gives a brief review of state-of-the-art WRONoC topologies. Section 3 introduces our  $4 \times 3$  router design and analyzes its performance regarding MRR usage, insertion loss and crosstalk noise. Section 4 presents the methods to build the  $N \times (N - 1)$  *Light* topology and to configure the MRR resonant wavelengths. We demonstrate the superiority of *Light* in energy efficiency, signal-to-noise ratio (SNR) and scalability with experimental results in Section 5.

## 2 STATE-OF-THE-ART WRONOC TOPOLOGIES

As introduced before, CSEs with two identical MRRs are the fundamental building blocks of many WRONoC topologies, such as  $\lambda$ -router [10], Snake [8] and GWOR [20].

Figure 3 shows the logic schemes of a  $4 \times 4$   $\lambda$ -router and a  $4 \times 4$  Snake. Both topologies can support all-to-all simultaneous communication among 4 masters and 4 slaves. For example, following the paths shown in Figure 3(a), master  $m_1$  can send data to slaves  $s_1$ ,  $s_2$ ,  $s_3$  and  $s_4$  at the same time with blue, green, red, and yellow lines, respectively. The CSEs in Snake shown in Figure 3(b) form a triangular structure which provides more flexible options for waveguide routing during physical implementation.

In  $\lambda$ -router and Snake, masters and slaves are placed at two distant ends of their logic schemes. However, in WRONoC applications,

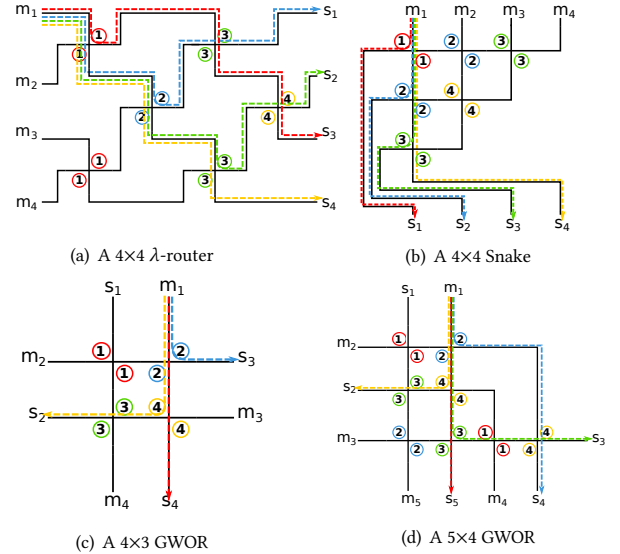


Figure 3: State-of-the-art WRONoC topologies

an IP-core usually acts as both the master and slave. Therefore, the positions of the master and the slave that represent the same IP-core should be close to each other. GWOR is a WRONoC topology that mostly matches this layout constraint. The only exception happens when the number of IP-cores is odd. In this case, exactly one master-slave pair will be separated from each other. Figure 3 shows two GWORs with 4 and 5 IP-cores, respectively. In Figure 3(d),  $m_3$  and  $s_3$  are separated from each other. In GWOR, each IP-core can communicate with all other IP-cores. This is a realistic assumption since for short-distance communication inside the same IP-core, it is more energy-efficient to use electronic links instead of optical links as the former do not require E/O and O/E conversions.

## 3 HASH: A NOVEL $4 \times 3$ WRONOC ROUTER

As introduced before, state-of-the-art WRONoC topologies suffer from scalability concerns due to their large MRR usage and the mismatch with physical layout constraints. To address these problems, we propose a novel  $4 \times 3$  WRONoC router: *Hash*, and analyze its performance regarding MRR usage, insertion loss and crosstalk.

### 3.1 Logic Scheme

As shown in Figure 4, Hash consists of four PSEs. Regardless of the parity of the number of IP cores, Hash always places the master and the slave of the same IP-core close to each other. Each IP-core in Hash can communicate with all other IP-cores except for itself. Figure 4 shows the signal paths reserved for  $m_1$ . Specifically, an optical signal from  $m_1$  will follow the waveguide connected to  $s_3$  until it is on-resonance with an MRR along that waveguide. Thus,  $m_1$  can send signals to  $s_2$  and  $s_4$  on wavelength  $\lambda_2$  and  $\lambda_1$  so that they will be on-resonance with the bottom left and the upper left MRRs, respectively. Since  $m_1$  is directly connected to  $s_3$ , it can communicate with  $s_3$  on any wavelength other than  $\lambda_1$  and  $\lambda_2$ . The matrix in Figure 4 shows the wavelengths used by all signal paths.

### 3.2 MRR Usage

With only four MRRs on two different resonant wavelengths, Hash supports concurrent communication between 12 master-slave pairs.

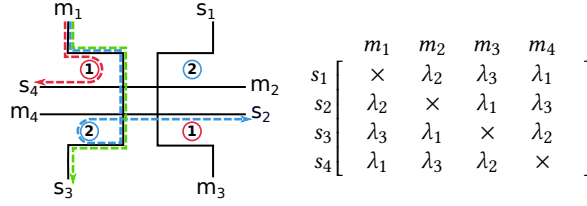


Figure 4: The logic scheme of Hash

We show that this is the smallest possible MRR usage under the condition that no additional waveguide is implemented. For the 12 signal paths, at least 4 waveguides are needed to connect a master to a slave. These waveguides can form 4 signal paths (the default paths) which do not rely on MRRs. There are 8 signal paths that need to be routed with MRRs. Since a CSE/PSE supports 2 different signal paths, at least 4 CSEs/PSEs are needed to support 8 signal paths. Compared to the CSEs with two MRRs in  $\lambda$ -router and GWOR, Hash uses the fewest MRRs to support the network with 4 IP-cores by using the PSEs.

### 3.3 Insertion Loss and Crosstalk Noise

The optical switch elements (OSEs) like PSEs and CSEs have inevitable crosstalk noise and insertion loss, which decrease the signal-to-noise ratio (SNR) and cause additional power penalty [21].

Without the physical implementation, the analysis of the insertion loss and crosstalk noise here considers *crossing loss*, *through loss* and *drop loss*.

For the noise signals, only the first-order noise generated by signals is taken into consideration. The second-order noise and the higher-order noise generated by the first-order noise signals or other noise signals are ignored. The output signal power and noise power in the crossing and PSEs are given in Table 1. Table 2 shows the coefficients of insertion loss and crosstalk [13].

Table 1: Output power and noise power in Crossing and PSEs

	(a) Crossing	(b) PSEs for off-resonance signals	(c) PSEs for on-resonance signals
Output power	$P_{Out1} = L_c P_{in}$	$P_{Through} = L_t P_{in}$	$P_{Drop} = L_d P_{in}$
Noise power	$P_{Out2} = P_{Out3} = K_c P_{in}$	$P_{Drop} = K_r P_{in}$	$P_{Through} = K_r P_{in}$

Table 2: Insertion loss coefficients and Crosstalk coefficients

Through loss ( $L_t$ )	Drop loss ( $L_d$ )	Crossing loss ( $L_c$ )
-0.005dB	-0.5dB	-0.04dB

Crosstalk per MRR ( $K_r$ )	Crosstalk per crossing ( $K_c$ )
-25dB	-40dB

We analyse the insertion loss and crosstalk noise in Hash based on the three types of signal paths:

1) Signals on **Type-I paths** directly pass through the waveguides and reach the slave ports without being coupled by any MRRs. For instance, the signal from  $m_1$  to  $s_3$ , represented by the green line in Figure 5(a), is not coupled with any MRRs along this waveguide. Other **Type-I paths** are  $m_2 \rightarrow s_4$ ,  $m_3 \rightarrow s_1$ , and  $m_4 \rightarrow s_2$ . The signal from  $m_1$  passes two off-resonance MRRs and two waveguide crossings to reach  $s_3$ . The output signal power at  $s_3$  can be calculated as

$$P_{signal,typ1} = L_c^2 L_t^2 P_I \quad (1)$$

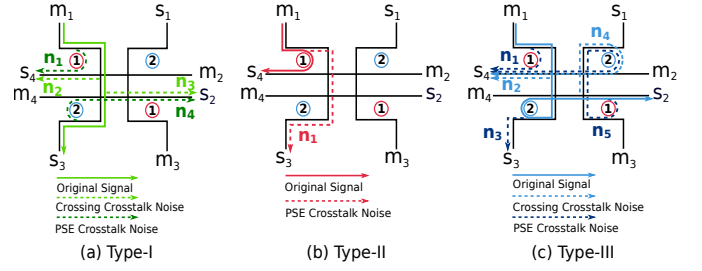


Figure 5: Crosstalk noise and insertion loss of different types of signal paths

and the insertion loss value of **Type-I paths** can be easily calculated as  $l_{typ1} = -2(L_c + L_t) = 0.09dB$ . The negative sign is added to indicate the insertion loss values ( $10\log(P_{input}/P_{output})$ ) rather than the insertion loss coefficients ( $10\log(P_{output}/P_{input})$ ).

The crosstalk noise signals generated by the signal from  $m_1$  to  $s_3$  are represented by  $n_1, n_2, n_3$  and  $n_4$  in Figure 5(a). The crosstalk signals are indexed according to the sequence in which they are encountered during the propagation of the desired signal. The noise signal power can be expressed as

$$P_{noise,typ1} = \left( \underbrace{K_r}_{n_1} + \underbrace{K_c L_t^2}_{n_2} + \underbrace{K_c L_t^2 L_c^2}_{n_3} + \underbrace{K_r L_t^2 L_c^4}_{n_4} \right) P_I \quad (2)$$

With the values in Table 2, the noise power generated by the Type-I signal paths at each slave is -21.90dB $\cdot P_I$ .

2) Signals on **Type-II paths** are coupled with the first MRR that they encounter in a Hash. For example, the signal from  $m_1$  to  $s_4$  carried by  $\lambda_1$ , represented by the red line in Figure 5(b), is coupled with the MRRs at the upper left, then switched to the waveguide connected to  $s_4$ . Other **Type-II paths** are  $m_2 \rightarrow s_1$ ,  $m_3 \rightarrow s_2$ , and  $m_4 \rightarrow s_3$ . In these paths, an optical signal is coupled with one MRR which generates the *drop loss* once. Thus the output signal power at  $s_4$  can be calculated as

$$P_{signal,typ2} = L_d P_I \quad (3)$$

and the insertion loss value of **Type-II paths** is  $l_{typ2} = -L_d = 0.5dB$ .

The first-order noise signal caused by path  $m_1 \rightarrow s_4$  is represented by the red dash line in Figure 5(b). The noise power can be calculated as

$$P_{noise,typ2} = (K_r L_t L_c^2) P_I \quad (4)$$

The noise power generated by **Type-II paths** is -25.16dB $\cdot P_I$ .

3) Signals on **Type-III paths** are coupled with the second MRR that they meet in a Hash, such as the  $m_1 \rightarrow s_2$  shown in Figure 5(c). Other **Type-III path** are  $m_2 \rightarrow s_3$ ,  $m_3 \rightarrow s_4$ , and  $m_4 \rightarrow s_1$ . The signal sent by  $m_1$  is coupled with the MRR at the lower left in the Hash and switched to the waveguide connected to  $s_2$ . In this case, the output power at  $s_2$  is

$$P_{signal,typ3} = (L_d L_t^2 L_c^4) P_I \quad (5)$$

The insertion loss value of those signal paths can also be expressed as  $l_{hash,typ3} = -(2L_t + L_d + 4L_c) = 0.67dB$ . The **Type-III path**  $m_1 \rightarrow s_2$  generates 5 noise signals shown by Figure 5(c). Among them,  $n_1, n_2, n_4$  and  $n_5$  go to  $s_4$ , while  $n_3$  goes to  $s_3$ . The noise power can be calculated as

$$P_{noise,typ3} = \underbrace{(K_r + K_c L_t^2 + K_c L_t^2 L_d^2 L_c^6)}_{n_1} + \underbrace{K_r L_t^2 L_d^2 L_c^8}_{n_2} + \underbrace{K_r L_t L_c^2}_{n_3} P_I \quad (6)$$

The noise power generated by **Type-III path** is  $-21.86\text{dB} \cdot P_I$ .

With the definition of SNR, the SNR is expressed as  $10 \log \frac{P_{output}^{\lambda n}}{P_{noise}^{\lambda n}}$ , where  $P_{output}$  denotes the output power of the desired signal and  $P_{noise}$  is the power of all crosstalk signals that have the same destination and wavelength as the desired signal. Hash increases the average SNR by 10% and 17% compared to a  $4 \times 3$   $\lambda$ -router and a  $4 \times 3$  GWOR, respectively. The advantages of Hash in SNR come from its lower MRR usage, as MRRs are major sources of crosstalk signals. Thus, the reduction of MRR usage benefits the signal quality.

## 4 LIGHT: A WRONOC TOPOLOGY BASED ON HASH

If we replace the masters and the slaves with inputs and outputs, a Hash can be considered as a complex optical switching element with 4 inputs and 4 outputs. With Hash as the basic building block, we can easily construct an  $N \times (N-1)$  WRONoC topology: *Light* for full communication among  $N$  IP-core except for self-communication.

### 4.1 Waveguide Connections

The structure of an  $N \times (N-1)$  *Light* is shown by Figure 6. In an  $N \times (N-1)$  *Light*,  $\lceil \frac{N}{2} \rceil (\lceil \frac{N}{2} \rceil - 1) / 2$  Hashes are needed; and this structure can be expanded to any sizes. The structure is formed by these steps:

1) Place  $\lceil \frac{N}{2} \rceil - 1 - (k-1)$  Hashes horizontally in  $k$ -th row with  $1 \leq k \leq \lceil \frac{N}{2} \rceil - 1$ . Connect the left ports of each Hash with its left neighbor.

2) Connect the bottom ports of Hash to its bottom neighbor except for the Hash at the rightmost end of each row. Connect the bottom ports of Hash at the rightmost end of each row to its bottom left neighbor.

3) Connect the upper ports of Hashes in the first row to the ports  $m_1, s_1, m_2, s_2, m_3, s_3, \dots, m_{\lceil \frac{N}{2} \rceil - 1}$  and  $s_{\lceil \frac{N}{2} \rceil - 1}$ , sequentially. If the number of IP-cores is even, then connect the right ports of the Hash at the rightmost end in the first row to  $m_{\lceil \frac{N}{2} \rceil}$  and  $s_{\lceil \frac{N}{2} \rceil}$ .

4) Connect the left ports of Hashes in the first column to ports  $m_N, s_N, m_{N-1}, s_{N-1}, \dots, m_{\lceil \frac{N+1}{2} \rceil + 2}, s_{\lceil \frac{N+1}{2} \rceil + 2}, m_{\lceil \frac{N+1}{2} \rceil + 1}, s_{\lceil \frac{N+1}{2} \rceil + 1}$ , sequentially. Connect the bottom input and output of Hash in the last row to  $m_{\lceil \frac{N+1}{2} \rceil}$  and  $s_{\lceil \frac{N+1}{2} \rceil}$ .

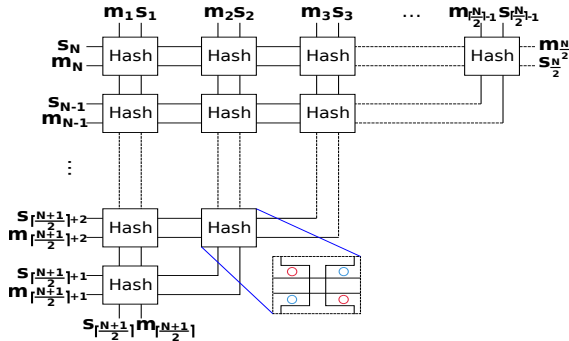


Figure 6: The  $N \times (N-1)$  *Light* structure

## 4.2 Wavelength Assignment

Each Hash contains two different wavelengths, which can be regarded as a wavelength-set ( $\Lambda$ ). For example, in the Hash shown in Figure 4, the wavelength-set  $\Lambda_1$  contains  $\lambda_1$  and  $\lambda_2$  ( $\Lambda_1 = \{\lambda_1, \lambda_2\}$ ). In this case, the task to assign wavelengths to each MRR is converted into the task to assign a wavelength-set to each Hash. To assign wavelengths to MRRs, two important rules need to be obeyed to avoid data-collision: [18]

- 1) Wavelengths assigned to the signal paths between the same *masters* and different *slaves* must be different;
- 2) Wavelengths assigned to the signal paths between different *masters* and the same *slaves* must be different.

Based on these two rules, we propose a simple resonant wavelength configuration approach to address the wavelength assignment problem. For an  $N \times (N-1)$  *Light*, we first construct a  $(\lceil \frac{N}{2} \rceil - 1) \times (\lceil \frac{N}{2} \rceil - 1)$  *Wavelength-set Matrix*, where each entry represents a wavelength-set ( $\Lambda$ ). After that, we fill the matrix column by column by repeatedly iterating over an array from 1 to  $\lceil \frac{N}{2} \rceil$ . At last, we configure the Hashes according to the matrix.

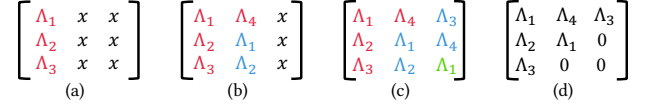


Figure 7: Wavelength-set assignment for an  $8 \times 7$  topology

For example, to configure the resonant wavelengths of MRRs in an  $8 \times 7$  *Light* topology, we first construct a  $3 \times 3$  *Wavelength-set matrix* and 4 wavelength-sets  $[\Lambda_1, \Lambda_2, \Lambda_3, \Lambda_4]$ . We fill the first column with  $\Lambda_1, \Lambda_2$ , and  $\Lambda_3$  as shown in Figure 7(a) and fill  $\Lambda_4$  to the first entry in the second column. Then we begin the second iteration from  $\Lambda_1$  again and fill  $\Lambda_1, \Lambda_2$  to the remaining two entries in the second column shown in Figure 7(b). After repeating this step again for the third column, we have a filled  $3 \times 3$  *Wavelength-set matrix* shown in Figure 7(c). Since only 6 Hashes are required for this topology, the entries below the counter-diagonal are replaced by 0 shown in Figure 7(d).

We configure the MRRs of the  $8 \times 7$  *Light* with the  $3 \times 3$  *Wavelength-set matrix* shown in Figure 7(d). Assume that  $\Lambda_1 = (\lambda_1, \lambda_2)$ ,  $\Lambda_2 = (\lambda_3, \lambda_4)$ ,  $\Lambda_3 = (\lambda_5, \lambda_6)$ ,  $\Lambda_4 = (\lambda_7, \lambda_8)$ , the  $8 \times 7$  *Light* topology is presented by Figure 8. Specifically, the wavelength of a signal path, which a master is directly connected to a slave by a waveguide, can be configured with any wavelengths except for the resonant wavelengths of MRRs along the waveguide. However, the wavelength of the signal path, which a master and a slave are connected by two different waveguides, should be set as the the resonant wavelength of the MRR in the PSE that is formed with two waveguides.

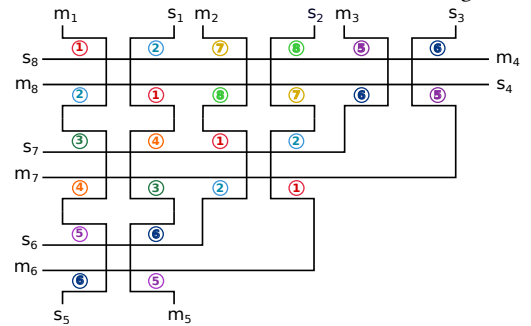


Figure 8: An  $8 \times 7$  *Light* topology

## 5 ANALYSIS AND COMPARISON

To evaluate the performance of *Light*, we compare *Light* with the state-of-the-art WRONoC topologies,  $\lambda$ -router, GWOR, and Snake, in terms of MRR usage, insertion loss, and SNR.

### 5.1 MRR Usage

In an  $N \times (N - 1)$  *Light*, there are  $\lceil \frac{N}{2} \rceil (\lceil \frac{N}{2} \rceil - 1) / 2$  Hashes, namely  $2 \lceil \frac{N}{2} \rceil (\lceil \frac{N}{2} \rceil - 1)$  MRRs, since each Hash has 4 MRRs. An  $N \times N$   $\lambda$ -router consists of  $N \lceil \frac{N}{2} \rceil + (N - 1) \lfloor \frac{N}{2} \rfloor$  CSEs with 2 MRRs, namely  $2(N \lceil \frac{N}{2} \rceil + (N - 1) \lfloor \frac{N}{2} \rfloor)$  MRRs. An  $N \times (N - 1)$  GWOR consists of  $N(N - 2)$  MRRs [20]. We compare the number of MRRs in *Light* to  $\lambda$ -router and GWOR for networks with more than 4 IP-cores.

Table 3: MRR usage in Routers

	Number of IP-cores				
	4	8	16	32	64
MRR usage in Snake	12	-	-	-	-
MRR usage in $\lambda$ -router	12	112	240	992	4032
MRR usage in GWOR	8	48	224	960	3968
MRR usage in <i>Light</i>	4	24	112	480	1984

Table 3 presents the MRR usage in *Light*,  $\lambda$ -router, GWOR, and Snake for different sizes of networks. Compared to these topologies that employ CSEs, *Light* reduces the number of MRRs by more than half. This reduction is achieved because *Light* replaces CSEs with PSEs which route two signals with one MRR. The reduction in MRR usage has multiple benefits. First, fewer MRRs indicate less MRR tuning power. As proposed in a recent survey paper [17], depending on the number of MRRs in the topology, MRR tuning power contributes 20-60% to the total optical power. Second, MRRs are important sources of crosstalk noise which negatively correlates with the SNR.

### 5.2 Insertion Loss

We calculated the *drop loss*, *through loss* and *crossing loss* in *Light*,  $\lambda$ -router, Snake, and GWOR with parameter values in Table 2. We removed the self-communications in the  $\lambda$ -router and Snake for a fair comparison. For the network with 4 IP-cores, the values of average insertion loss and worst-case loss in these topologies are given by Table 4. For this small network, all topologies perform similarly in both average and worst-case insertion losses.

Table 4: Insertion loss in 4x3 Routers

	$\lambda$ -router	Snake	GWOR	<i>Light</i>
Avg. Loss/dB	0.45	0.45	0.4	0.42
Worst-case Loss/dB	0.65	0.65	0.6	0.67

For large networks with more than 4 IP-cores, Figure 9 shows the average and worst-case insertion loss values in *Light*,  $\lambda$ -router and GWOR. In general, *Light* outperforms  $\lambda$ -router in the average insertion loss, but suffers more worst-case insertion loss. For example, in the network with 64 IP-cores, the average insertion loss of *Light* is 8.8% less than the average loss of  $\lambda$ -router and 7.4% less than the average loss of GWOR. Although GWOR and *Light* have greater worst-case insertion loss than  $\lambda$ -router, both topologies can match their physical layouts better than  $\lambda$ -router. In physical implementation, the additional crossings or long detours in  $\lambda$ -router result in more propagation loss or crossing loss which increases the insertion loss. The analysis of insertion loss involving propagation loss and bending loss in  $\lambda$ -router and *Light* is given in Section 5.4.

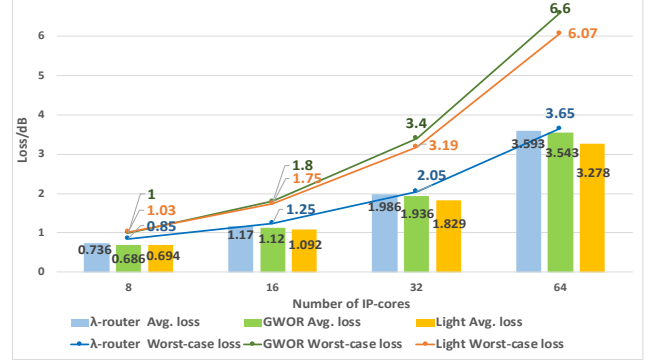


Figure 9: Average and worst-case loss in *Light*,  $\lambda$ -router and GWOR

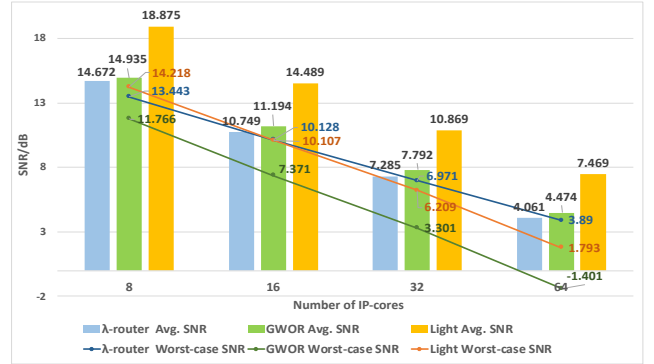


Figure 10: Average and worst-case SNR in *Light*,  $\lambda$ -router, and GWOR

### 5.3 Signal-to-Noise Ratio (SNR)

To evaluate the signal quality in *Light*, we calculated the SNR in  $\lambda$ -router, Snake, GWOR and *Light* for the network with 4 IP-cores. In a 4x3 GWOR shown in Figure 3(c), the signals, coupled with the first MRR they encounter, have no noise signals so that their SNR values are infinite. We remove these 4 signal paths and calculate the average SNR for the remaining 8 signal paths. The results given in Table 5 show that *Light* has both greater average SNR value and worst-case SNR than other topologies.

Table 5: SNR in 4x3 Routers

	$\lambda$ -router	Snake	GWOR	<i>Light</i>
Avg. SNR/dB	20.117	20.116	18.8879	22.1115
Worst-case SNR/dB	17.1445	16.9714	18.8707	19.9019

We compared the SNR in *Light*,  $\lambda$ -router and GWOR for the network with  $N$  IP-cores, where  $N = 8, 16, 32, 64$ . For  $N \geq 4$ , in GWOR, 3 signals with no noise have infinite SNR values. We remove them to calculate the average SNR. The results in Figure 10 show that *Light* outperforms  $\lambda$ -router and GWOR in the average SNR, particularly for large networks. For example, in the network with 64 IP-cores, *Light* increases the average SNR by 83.9% and 66.9% compared to  $\lambda$ -router and GWOR, respectively. For worst-case SNR, both *Light* and GWOR have lower worst-case SNR than  $\lambda$ -router, but *Light* increases the worst-case SNR compared to GWOR.

We analyzed the SNR of each signal path in *Light*,  $\lambda$ -router, and GWOR for a network with 32 IP-cores. The total 992 paths in  $\lambda$ -router have similar SNR values (7dB) smaller than the average SNR of *Light*, while 91% paths in *Light* have larger SNR than 7dB. This

observation demonstrates great potential of *Light* in application-specific WRONoCs, where some signal paths are not required [14]. The removal may not benefit  $\lambda$ -router too much, because of the similar SNR values. But for *Light*, this removal may significantly reduce the insertion loss, if we can smartly pick out the signal paths that suffer the most insertion losses to be removed. *Light* has a large range of insertion loss due to the arrangement of the positions of master/slave nodes. Although GWOR has a similar arrangement as *Light* when the number of IP-cores is even, 880 (89%) paths in 32×31 GWOR achieve smaller SNR values than the average SNR of *Light*. Benefiting from the reduced MRR usage, the crosstalk noise is less severe in *Light* than in GWOR, which contributes to the significant advantages of *Light* in SNR.

#### 5.4 Physical Implementation

As introduced before, each IP-core acts as both master and slave, and hence the master and slave ports are close to each other in reality. Based on such physical constraints, we manually design  $\lambda$ -router and *Light* for a network with 8 IP-cores in a 1.6cm × 1.6cm chip. For both layouts, we try to minimize the lengths of waveguides under the condition that no additional waveguide crossings will be introduced, and we place both topologies as centralized routers on the middle of the chip as shown in Figure 11(a) and Figure 11(b).

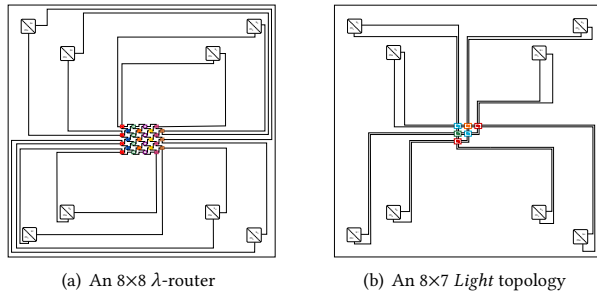


**Figure 11: Physical layouts for  $\lambda$ -router and *Light* topology**

According to these physical layouts, we calculated the insertion loss including the *propagation loss* (0.274dB/cm) and *bending loss* (0.005dB/90°) in  $\lambda$ -router and *Light* [13].

**Table 6: Physical features in both physical layouts**

Physical feature	$\lambda$ -router	<i>Light</i>
#crossings in CSEs or Hashes	28	24
#bending	139	90
Length of waveguides (total)	25.6cm	17.7cm
Length of waveguides (worst*)	4.16cm	2.50cm
Insertion loss (total)	48.91dB	44.17dB
Insertion loss (worst*)	2.09dB	1.82dB

worst\*: the signal path that has the worst-case insertion loss.

Table 6 shows the physical features in both physical layouts. Thanks to the realistic model of the positions of nodes, *Light* connects the master and the slave from the same IP-core to a pair of neighboring input and output without detouring. With this arrangement *Light* reduces the total waveguide lengths by 31% compared to  $\lambda$ -router. However, the long detours in  $\lambda$ -router, which are inevitable to avoid additional crossings, result in much propagation loss. Compared to  $\lambda$ -router, *Light* reduces the total insertion loss by 10% and the worst-case loss by 13%. Thus, in physical implementation, *Light* outperforms  $\lambda$ -router in both average insertion loss and worst-case insertion loss. The reduction of insertion loss in *Light* benefits the further enhancement of signal quality.

## 6 CONCLUSION

In this work, we proposed a novel WRONoC topology: *Light*. With a novel 4×3 router structure as the fundamental building block and a simple resonant wavelength configuration approach, *Light* can easily be implemented to support  $N \times (N - 1)$  communication at any scale. According to the comparison between *Light* and typical state-of-the-art WRONoC topologies, *Light* reduces the MRR usage by more than half and avoids additional waveguide crossings or detours during physical implementation. Based on a detailed analysis, we concluded that *Light* outperforms  $\lambda$ -router and GWOR in average insertion loss value and average SNR value. Furthermore, *Light* has great potential in application-specific WRONoCs. By removing the few signal paths with high insertion loss or low SNR, the network performance will be further improved.

## ACKNOWLEDGMENTS

This work is supported by the Deutsche Forschungsgemeinschaft (DFG, German Research Foundation) – Project Number 439798838.

## REFERENCES

- [1] A. Truppel et al. 2020. PSION+: Combining logical topology and physical layout optimization for Wavelength-Routed ONoCs. *IEEE Transactions on Computer-Aided Design of Integrated Circuits and Systems* (2020), 1–1.
- [2] C. Manolatos et al. 2002. *Passive Components for Dense Optical Integration*. Springer.
- [3] D. Vantrease et al. 2008. Corona: System Implications of Emerging Nanophotonic Technology. *ACM SIGARCH Computer Architecture News* 36, 3 (2008), 153–164.
- [4] Koohi et al. 2012. Scalable architecture for a contention-free optical network on-chip. *J. Parallel and Distrib. Comput.* 72, 11 (2012), 1493–1506.
- [5] L. Duong et al. 2014. A case study of signal-to-noise ratio in ring-based optical networks-on-chip. *IEEE Design & Test* 31, 5 (2014), 55–65.
- [6] L. Ramini et al. 2012. Engineering a Bandwidth-Scalable Optical Layer for a 3D Multi-core Processor with Awareness of Layout Constraints. In *IEEE/ACM International Symposium on Networks-on-Chip (NoCS)*. 185–192.
- [7] L. Ramini et al. 2012. Power efficiency of wavelength-routed optical NoC topologies for global connectivity of 3D multi-core processors. In *Proceedings of the Fifth International Workshop on Network on Chip Architectures*. 25–30.
- [8] L. Ramini et al. 2013. Contrasting Wavelength-Routed Optical NoC Topologies for Power-Efficient 3D-Stacked Multicore Processors using Physical-Layer Analysis. 1589–1594.
- [9] L. Zhang et al. 2014. On reducing insertion loss in wavelength-routed optical network-on-chip architecture. *IEEE/OSA Journal of Optical Communications and Networking* 6, 10 (2014), 879–889.
- [10] M. Briere et al. 2007. System Level Assessment of an Optical NoC in an MPSoC Platform. 1084–1089.
- [11] M. Li et al. 2018. CustomTopo: A Topology Generation Method for Application-Specific Wavelength-Routed Optical NoCs.
- [12] M. Li et al. 2020. Maximizing the Communication Parallelism for Wavelength-Routed Optical Networks-On-Chips. In *2020 25th ASP-DAC*. IEEE, 109–114.
- [13] M. Nikdast et al. 2015. Crosstalk Noise in WDM-Based Optical Networks-on-Chips: A Formal Study and Comparison. *IEEE Transactions on VLSI Systems* 23, 11 (2015), 2552–2565.
- [14] S. Le Beux et al. 2013. Reduction methods for adapting optical network on chip topologies to 3D architectures. *Microprocessors and Microsystems: Embedded Hardware Design* 37, 1 (2013), 87–98.
- [15] S. Le Beux et al. 2011. Layout guidelines for 3D architectures including optical ring network-on-chip (ORNOC). In *2011 IEEE/IFIP 19th International Conference on VLSI and System-on-Chip*. IEEE, 242–247.
- [16] S. Werner et al. 2015. Amon: An advanced mesh-like optical NoC. In *2015 IEEE 23rd Annual Symposium on High-Performance Interconnects*. IEEE, 52–59.
- [17] S. Werner et al. 2017. A survey on optical network-on-chip architectures. *ACM Computing Surveys (CSUR)* 50, 6 (2017), 1–37.
- [18] T. Tseng et al. 2019. Wavelength-Routed Optical NoCs: Design and EDA - State of the Art and Future Directions: Invited Paper. In *2019 IEEE/ACM ICCAD*. 1–6.
- [19] W. Bogaerts et al. 2012. Silicon microring resonators. *Laser & Photonics Reviews* 6, 1 (2012), 47–73.
- [20] X. Tan et al. 2011. On a Scalable, Non-Blocking Optical Router for Photonic Networks-on-Chip Designs. In *Symp. Photonics and Optoelectronics (SOPO)*.
- [21] Y. Xie et al. 2010. Crosstalk noise and bit error rate analysis for optical network-on-chip. 657–660.
- [22] B. Lin and C. Lea. 2012. Crosstalk Analysis for Microring Based Optical Interconnection Networks. *Journal of Lightwave Technology* 30, 15 (2012), 2415–2420.